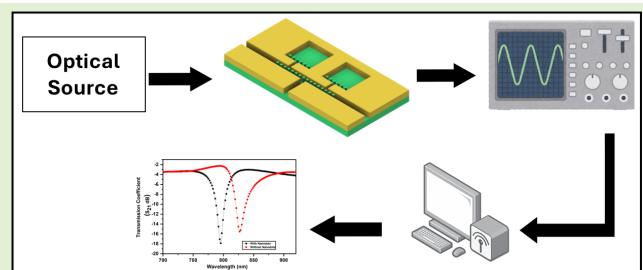


A Novel Plasmonic MIM Sensor Using Integrated 1×2 Demultiplexer for Individual Lab-on-Chip Detection of Human Blood Group and Diabetes Level in the Visible to Near-Infrared Region

Rummanur Rahad^{ID}, Member, IEEE, Mohammad Ashraful Haque^{ID}, Md. Omar Faruque^{ID}, Abu S. M. Mohsin^{ID}, Md Sadi Mobassir^{ID}, and Rakibul Hasan Sagor^{ID}

Abstract—In this article, we present an innovative plasmonic lab-on-chip (LoC) sensor featuring three ports, utilizing a 1×2 demultiplexer to detect two separate samples without cross-contamination. The performance of the sensor is numerically investigated using the finite element method (FEM), yielding a maximum sensitivity of 865.9 nm per refractive index unit (RIU) and a figure of merit (FOM) of 58.4 in the 700–920 nm range. The proposed metal–insulator–metal (MIM) structure, incorporating a diamond-shaped silicon nanodot array with a perimeter of less than 100 nm, serves as a sensing surface, detecting changes in the refractive index (RI) of the surrounding medium. Our suggested sensor demonstrates an extraordinary transmission coefficient (TC) of around –18-dB, it surpasses classical optics predictions, and its nanoscale light confinement enhances interaction with analytes. Our LoC sensor, based on the MIM structure, achieves high accuracy and precision in measuring small RI changes, making it portable and suitable for on-site applications, and settings with limited resources. This sensor streamlines medical processes by rapidly detecting blood groups and diabetes levels with minimal sample volume, potentially improving patient care efficiency.



Index Terms—Biosensor, demultiplexer, finite element method (FEM), lab-on-chip (LoC), metal–insulator–metal (MIM), silicon nanodot array, transmission coefficient (TC).

I. INTRODUCTION

OVER the last few years, optical biosensors have been a rapidly expanding field of research, with applications in various domains, such as health care, environmental monitoring, food safety, and biotechnology [1]. Label-free optical biosensors offer direct detection of biomolecules, addressing reliability concerns in label-based approaches. One of the

Manuscript received 8 February 2024; revised 27 February 2024; accepted 29 February 2024. Date of publication 8 March 2024; date of current version 16 April 2024. The associate editor coordinating the review of this article and approving it for publication was Dr. Barbara Adinolfi. (*Corresponding author: Rummanur Rahad.*)

Rummanur Rahad is with the IUT Photonics Research Group (IUTPRG), Department of Electrical and Electronic Engineering, Islamic University of Technology (IUT), Gazipur 1704, Bangladesh, and also with the Optics and Photonics Research Group, Department of Electrical and Electronic Engineering, BRAC University, Dhaka 1212, Bangladesh (e-mail: rummanurrahad@iut-dhaka.edu).

Mohammad Ashraful Haque, Md. Omar Faruque, Md Sadi Mobassir, and Rakibul Hasan Sagor are with the IUT Photonics Research Group (IUTPRG), Department of Electrical and Electronic Engineering, Islamic University of Technology (IUT), Gazipur 1704, Bangladesh.

Abu S. M. Mohsin is with the Optics and Photonics Research Group, Department of Electrical and Electronic Engineering, BRAC University, Dhaka 1212, Bangladesh.

Digital Object Identifier 10.1109/JSEN.2024.3372692

emerging areas of optical biosensor research is on-chip blood group detection and diabetes level monitoring. This can enable fast and automated blood grouping and monitoring of the diabetic condition in the human body, a vital procedure for blood transfusion and organ transplantation. Such technologies can enhance patient care in emergencies because of speed, automation, and portability. However, there are still challenges to overcome in terms of speed, automation, usability, and portability, and researchers are working to address these issues [2], [3].

In the realm of nanophotonics, researchers are focusing on exploring novel nanometallic structures, especially those that can produce plasmonic effects with advanced techniques. The key concept for this field is surface plasmon polaritons (SPPs), which explain how light and matter interact at the nanoscale [4]. SPPs, characterized by greater momentum than light, challenge conventional notions of light propagation, surpassing the diffraction limit and enabling the development of smaller, more compact optical components [37]. SPPs have many uses in various areas of technology, such as sensors, filters, Mach-Zehnder interferometers, splitters, and switches [35], [36]. SPPs can control light with high

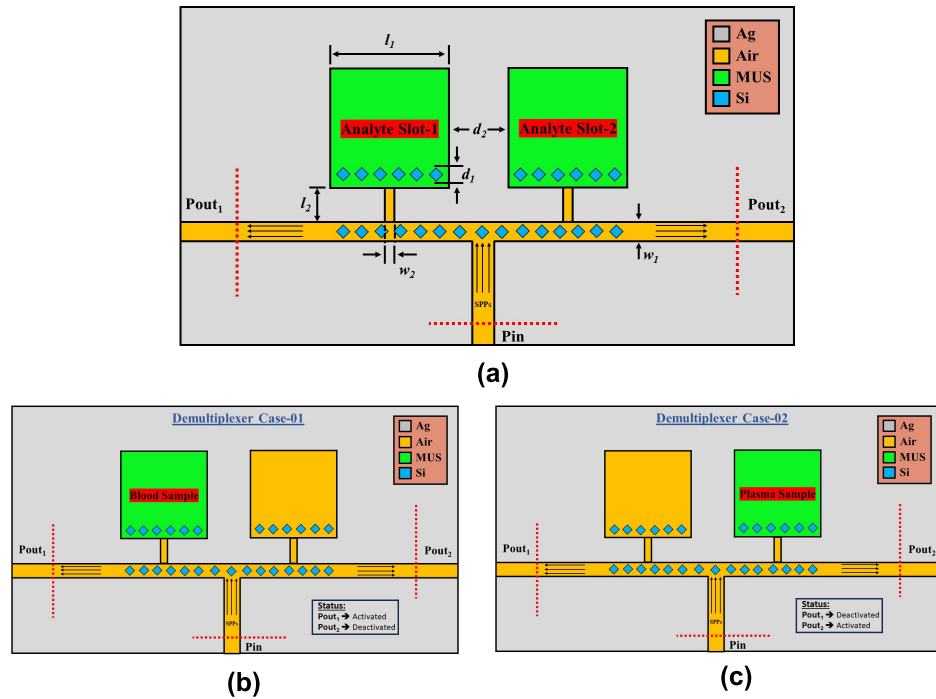


Fig. 1. (a) Schematic of the proposed LoC sensor. (b) Sensing mechanism for detection of analyte-1. (c) Sensing mechanism for detection of analyte-2.

precision, as they can localize, confine, and adjust it at subwavelength scales [38].

The metal–insulator–metal (MIM) waveguide-integrated plasmonic refractive index (RI) sensor is extensively employed in the detection of gases, liquids, temperature variations, material concentrations, and biological substances owing to its superior field confinement capabilities [5]. Despite the lower sensitivity of MIM structures compared to optical fiber sensors because of high ohmic losses, recent advancements involve coupling them with coupling with nanodisk resonators, ring cavities, nanodisc cavities, and nanodots to improve sensitivity through plasmon resonance [6], [7], while maintaining other performance parameters. Researchers are dedicated to advancing nanoscale-integrated MIM sensors, with a primary focus on improving capabilities for applications like glucose sensing, photothermal therapy, monitoring diabetes levels, and the identification of diseases [5]. Chen et al. [31] proposed a CRISPR-empowered SPR platform, that swiftly detects SARS-CoV-2 variants, including Omicron, with high sensitivity in 38 min, offering a cost-effective solution for precise mutation identification. Zheng et al. [32] proposed a graphdiyne-based CRISPR-SPR-Chip that swiftly detects gene mutations without amplification, providing a breakthrough in on-chip clinical gene analysis in just 5 min. Xue et al. [33] investigated an antimonide-based SPR sensor that achieves label-free, ultrasensitive detection of cancer-related microRNAs (miRNA-21 and miRNA-155) with a 10 aM detection limit, promising breakthroughs in early cancer diagnosis. Chen et al. [34] suggested an MXene-AuNP biosensor with CRISPR/Cas13a that enables rapid, ultrasensitive detection and distinction of SARS-CoV-2 variants, including Omicron BA.5 and BA.2, supplementing RT-qPCR for early diagnosis and variant identification. Butt et al. [9] developed a plasmonic sensor based

on a MIM waveguide, capable of analyzing various samples, including blood, urine, and other bodily fluids, for the diagnosis of diseases or conditions. However, using multiple analytes may compromise the accuracy and efficiency of the analysis due to the risk of contamination [10]. Moreover, using multiple single-path sensors for different analytes comes with more manufacturing and fabrication costs. To tackle this issue, we are proposing a single sensor that greatly minimizes the fabrication cost of the devices.

In this article, we present a plasmonic MIM sensor that incorporates a 1×2 demultiplexer, and it can measure two blood analytes (red blood cell (RBC) and glucose) without cross-contamination and determine the blood group and diabetes level of the sample. By optimizing the structural parameters, we achieved a sensitivity of 865.9 nm/RIU and a figure of merit (FOM) of 58.4 in the visible to near-infrared (NIR) region. Our sensor also has a high detection limit of 1.1548×10^{-6} RIU, and this feature makes our sensor suitable for point-of-care detection of blood groups and diabetes levels. The key component of our sensor is a diamond-shaped silicon nanodot array that enhances the light-matter interaction and increases the transmission coefficient (TC) (S_{21} dB).

II. LOC SENSOR DESIGN AND THEORETICAL ANALYSIS

As shown in Fig. 1(a), the proposed lab-on-chip (LoC) sensor consists of a MIM structure with three ports: Pin (input), P_{out1} , and P_{out2} (output). The biosensor can measure two analytes using the demultiplexing feature, which activates only one output port at a time and keeps the other port off. In our LoC sensor, when P_{out1} is activated, the scattering boundary condition is applied to P_{out2} , which is why only P_{out1} will function at that time. Similarly, P_{out2} also operates in the same way. Fig. 1(b) and (c) show the top views for the detection

process of analyte-1 and analyte-2, respectively, in which one cavity is filled with the material under sensing (MUS) and the other cavity is filled with air, and the optical output is taken from the corresponding output port. Our selection of two square-shaped resonators for the plasmonic MIM sensor with a 1×2 demultiplexer stems from its practical fabricability [39] and inherent symmetry. The symmetric design ensures identical results in both ports, simplifying resonance detection and reducing overall complexity. This choice optimizes performance while maintaining ease of fabrication, aligning with our objectives for practical application and efficiency. The metallic layer of the LoC sensor consists of silver (Ag), labeled as gray, and is modeled using the Johnson and Christy model [15]. Silver (Ag) is preferred over gold (Au) as the active plasmonic material for enhanced sensitivity and selectivity in optical and sensing applications due to its narrower resonance curve, leading to a smaller full width at half maximum (FWHM) [1]. That is why, it enhances the DA of the LoC sensors. Moreover, Ag has lower ohmic loss and lesser bandwidth than other noble metals, which results in enhanced field penetration [11]. However, Ag is susceptible to oxidation [40], which can compromise sensor performance and reliability over time. The sky color represents the diamond-shaped Si nanodot array, which is strategically integrated into the sensor to optimize the route of SPPs. The nanodots increase the interaction of SPPs with analyte molecules and amplify the evanescent field, leading to heightened sensitivity to minuscule environmental changes [12]. The simulation and optimization methods make use of the frequency domain (ewfd) features of the COMSOL Multiphysics software. To simulate the proposed sensor in 2-D, the finite element method (FEM) is used, with triangular extra fine meshing of 3146 domain elements and 461 border elements. These borders are defined as scattering boundaries to reduce reflection. The choice of 2-D geometry in simulation for a plasmonic MIM sensor is preferred over 3-D due to its faster computational speed, reduced storage requirements, and accurate representation of 3-D scenarios, especially when device height exceeds 800 nm, leading to optimized performance and efficiency without the need for computationally expensive 3-D simulations [41]. For our sensor, the real and imaginary components of the effective RI are shown in Fig. 2 for different heights of the sensor ranging from 100 to 1000 nm. It is evident that when the height is greater than 600 nm, the $\text{Re}(n_{\text{eff}})$ reaches a stable value which indicates that the 2-D and 3-D simulations provide similar results. Fig. 3(a) shows the observed rise in TC within the MIM structure with the presence of Si nanodot arrays, whereas Fig. 3(b) depicts the electric field. This increased TC is attributed to tunneling caused by the stimulation of resonant SPPs through the LoC structure. For our proposed sensor, the optimized parameters are $l_1 = 400$ nm, $l_2 = 100$ nm, $w_1 = 50$ nm, $w_2 = 10$ nm, $d_1 = 20\sqrt{2}$ nm, and $d_2 = 155$ nm.

The suitable method for making the suggested LoC sensor is electron beam lithography (EBL), which can create fine patterns without using masks. EBL offers sub-10 nm resolution, allowing for custom pattern creation, but its low throughput confines its application to photomask fabrication, low-volume semiconductor production, and research and development,

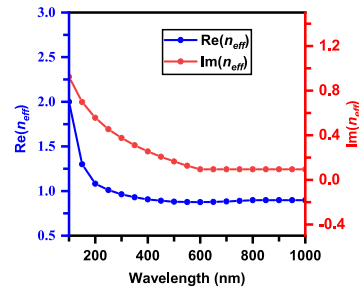


Fig. 2. Real and imaginary parts of the effective RI for different heights of the sensor.

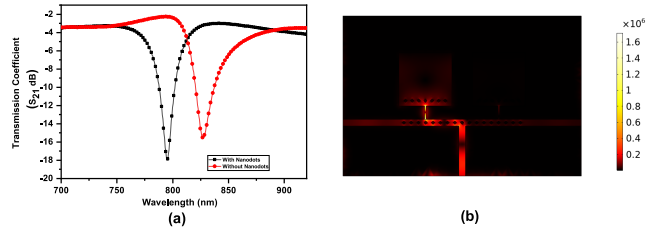


Fig. 3. (a) Effect of nanodots on the TC (S_{21} dB). (b) Normalized electric field (V/m) at the resonant wavelength.

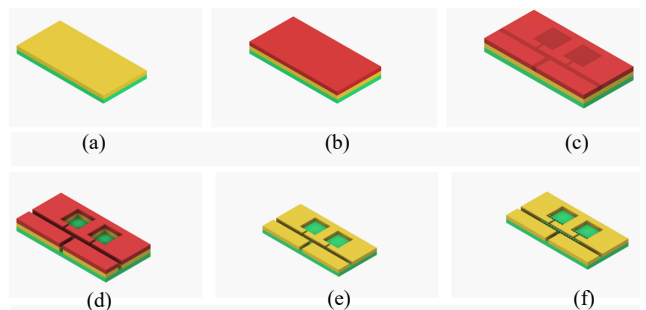


Fig. 4. EBL fabrication process for the proposed LoC sensor. (a) Ag deposition substrate. (b) EBL resist coating. (c) Pattern transfer using electron beam. (d) Chemical development and Reactive-ion etching. (e) Resist removal. (f) Sensor finalization.

making it ideal for intricate and unconventional shapes. Ag is initially deposited onto a Si substrate through remote plasma-enhanced atomic layer deposition (PALD) or magnetron sputtering [14]. Subsequently, an EBL resist is applied, exposing the resist to an electron beam to create a desired pattern. The exposed areas are chemically developed, followed by Ag etching and resist removal, achieving the final pattern on the substrate, and creating Si nanodots array on the Si substrate [13]. The illustration of the suggested fabrication process for the proposed LoC sensor is shown in Fig. 4.

The required condition of stimulation of SPPs in an Ag-Analyte interaction is [20]

$$\Re(\epsilon_{\text{Analyte}}) \times \Re(\epsilon_{\text{Ag}}) + \Im(\epsilon_{\text{Analyte}}) \times \Im(\epsilon_{\text{Ag}}) < 0. \quad (1)$$

Plasmonic sensors rely on SPPs for detecting RI changes in analytes at the metal-dielectric interface, and the dispersion relation of the MIM waveguide supports the fundamental transverse magnetic mode (TM_0) mode, which can be

expressed by the following equation [16]:

$$\tanh\left(\frac{k_{\text{Analyte}} \times W_1}{2}\right) = -\frac{\epsilon_{\text{Analyte}} \times k_{\text{Ag}}}{\epsilon_{\text{Ag}} \times k_{\text{Analyte}}}.$$
 (2)

Here, W_1 is the width of the MIM waveguide where ($W_1 \ll \lambda_{\text{incident}}$), k_{Analyte} , and k_{Ag} are wave vectors for analyte and Ag. The wave vectors can be defined as using conservation of momentum [17]

$$k_{\text{Analyte}} = \sqrt{\beta^2 - \mu_{\text{Analyte}} \times \epsilon_{\text{Analyte}} \times k_{\text{free space}}^2}$$
 (3)

$$k_{\text{Ag}} = \sqrt{\beta^2 - \mu_{\text{Ag}} \times \epsilon_{\text{Ag}} \times k_{\text{free space}}^2}$$
 (4)

here, $k_{\text{free space}}$ is the wave vector in free space which can be defined as, free space = $(\omega/c) = (2\pi)/\lambda$ and β is the propagation constant which can be defined as $\beta = n_{\text{eff}} k_{\text{free space}}$ where n_{eff} is the effective RI. The variation of the n_{eff} for the primary TM mode within the MIM waveguide can be investigated with respect to wavelength. The guided wavelength in the MIM waveguide (λ_{SPP}) is determined by the real component of the effective RI, while the propagation length of SPPs ($L_{\text{SPP}} = 1/(2\text{Im}(\beta))$) is influenced by its imaginary part. Consequently, the characterization of the n_{eff} can be articulated in the following manner [19]:

$$n_{\text{eff}} = \frac{\beta}{k} = \frac{\lambda}{\lambda_{\text{SPP}}} + j\left(\frac{\lambda}{4\pi \times L_{\text{SPP}}}\right)$$
 (5)

$$n_{\text{eff}} = \sqrt{\epsilon_{\text{Analyte}}} \sqrt{\epsilon_{\text{Analyte}} + \frac{\lambda \epsilon_{\text{Analyte}}}{W_1 \pi \sqrt{-\epsilon_{\text{Ag}}}} \sqrt{1 - \frac{\epsilon_{\text{Analyte}}}{\epsilon_{\text{Ag}}}}}.$$
 (6)

The unique quality factor of SPPs, denoted as Q_{SPP} , can be determined for a specific geometry, with a general limiting case providing insight into the material's overall Q_{SPP} , as expressed in the following equation [22]:

$$Q_{\text{SPP}} = \frac{\left[\epsilon'_{\text{Ag}}(\omega)\right]^2}{\epsilon''_{\text{Ag}}(\omega)}.$$
 (7)

The normalized SPP wavelength ($\lambda_{\text{SPP}}/\lambda_0$) can be calculated by the following expression [23]:

$$\frac{\lambda_{\text{SPP}}}{\lambda_0} = \sqrt{\frac{\epsilon_{\text{Analyte}} + \epsilon'_{\text{Ag}}}{\epsilon_{\text{Analyte}} * \epsilon'_{\text{Ag}}}}.$$
 (8)

The confinement of SPPs on the Ag-analyte interface is evident in the normalized SPP, where the SPP wavelength is shorter than the corresponding free space wavelength. When light is given as input, an electromagnetic wave travels from the input port to the output port, coupling with the resonator and generating the resonant wavelength (λ_{res}) according to the standing wave theory [45]

$$\lambda_{\text{res}} = \frac{2 * \text{Re}(n_{\text{eff}})L}{m - \frac{\phi_{\text{ref}}}{\pi}}$$
 (9)

where L is the effective length of the LoC sensor, m is a positive integer, and ϕ_{ref} is the phase shift. Here, $\text{Re}(n_{\text{eff}})$ changes based on the waveguide structure, material properties, and operating wavelength.

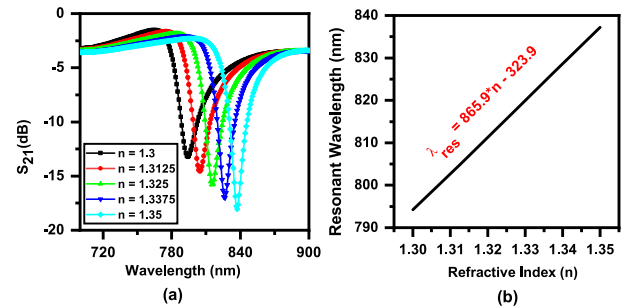


Fig. 5. (a) TC (S_{21}) of the sensor for different values of RI of the analyte. (b) Relation between resonant wavelength (λ_{res}) and RI of the analyte.

III. RESULT ANALYSIS AND APPLICATIONS

We studied the relationship of λ_{res} and RI (n), by varying n from 1.3 to 1.35 in steps of 0.0125, while keeping all the geometrical parameters fixed. As shown in Fig. 5(a) and (b), λ_{res} shifts to longer wavelengths as n increases, in agreement with 9. The resonance dip is very sensitive to n changes, and the wavelength shift can be precisely computed. This makes our LoC sensor ideal for sensing applications. The assessment of the sensor's effectiveness relies on a key metric called sensitivity (S), characterized by the relationship between the shift in wavelength ($\Delta\lambda$) and the corresponding change in RI (Δn) [9]

$$S = \frac{\Delta\lambda}{\Delta n}.$$
 (10)

The detection accuracy (DA) of a sensor measures the sharpness of the resonance dip and is calculated as the reciprocal of the FWHM [1]

$$\text{DA} = \frac{1}{\text{FWHM}}.$$
 (11)

Another important parameter is the FOM which indicates how easily the analyte can be detected and can be expressed by the following equation [24]:

$$\text{FOM} = \lambda_{\text{res}} \times \text{DA}.$$
 (12)

The detection limit (DL) of the LoC sensor can be calculated by the following equation:

$$\text{DL} = \frac{\delta\lambda}{S}$$
 (13)

where $\delta\lambda$ is the minimum changes of λ_{res} that can be identified by the optical spectrum analyzer (OSA) device. Typically, the resolution of commercial analyzers is 0.001 nm [21].

As our configuration is symmetric, that is why, we obtained the same performance metrics for both P_{out1} and P_{out2} . As shown in Fig. 1, the proposed sensor has the following performance parameters: S is 865.9 nm/RIU, DA is 0.0674 nm^{-1} , FOM is 58.4 RIU^{-1} , and DL is $1.1548 \times 10^{-6} \text{ RIU}$. Our sensor achieves a higher resolution because of the enhanced evanescent field, which allows the sensor to sense tiny variations in λ_{res} . We compare the performance metrics of our structure with other plasmonic sensors for blood analysis that have been reported in the literature, as shown in Table I.

TABLE I
COMPARISON OF PERFORMANCE WITH REPORTED WORKS

Ref.	Configuration	Analyte	Sensitivity (nm/RIU)	Operating Range (nm)	Demuxing
[27]	Photonic Crystal Waveguide	Blood	45.33	1384.5-1388	✗
[28]	Photonic Crystal Fiber	Blood	66.46	700-1400	✗
[29]	Photonic Crystal Waveguide	Blood	51.49	800-1200	✗
[30]	Photonic Crystal Biosensor	Blood	75	-	✗
[1]	MIM Waveguide	Blood	101.16	700-800	✗
This work	MIM Waveguide	Blood	865.9	700-920	✓

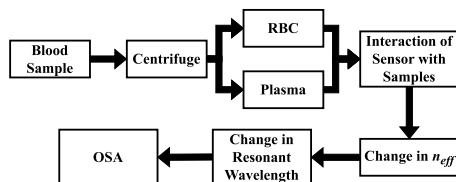


Fig. 6. Working process diagram of the LoC sensor.

The experimental setup consists of an optical sensor that operates in the visible and NIR spectrum, and a quantum cascade laser (QCL) that serves as the input optical source [42]. The QCL is connected to a single-mode fiber (SMF) that delivers the light to the input port of the LoC sensor. The cavity of the sensor contains the analyte, which is the substance to be measured. The analyte affects the n_{eff} of the cavity, which in turn determines the λ_{res} of the LoC sensor. When the QCL is turned on, the LoC sensor detects the change in λ_{res} due to the change in n_{eff} caused by the analyte, and the output port of the sensor is connected to another SMF that carries the light to an optical spectral analyzer that measures the λ_{res} [43]. The output ports of the sensor are connected to the OSA. $P_{\text{out}1}$ will be connected to input channel 1 of the OSA, and $P_{\text{out}2}$ will be connected to another channel of the OSA. So, the output graph for the detection of the blood group will always appear at channel 1 output and the output graph for the detection of glucose concentration will always appear at channel 2 output of the OSA. For the sensing purpose of our demultiplexer-based LoC sensor, we have to isolate suitable samples (RBC and glucose) from the blood using a sequential method of centrifugation, purification, molecular separation, and concentration enhancement. Then, we apply ultrafiltration and nanofiltration to the plasma and hemoglobin, separated from the blood-anticoagulant mixture, to selectively separate glucose and RBC [5]. The size of the analyte is within the sensor's acceptable range at this point. Using nanopipettes, which are extremely small diameter pipettes at the nanoscale, the targeted delivery of analytes to specific resonator cavities [44] are enabled. We then inject the purified and concentrated solution into the cavities of the proposed sensor to detect changes in n_{eff} and λ_{res} , which allow us to observe the TC, and measure the concentration based on RI. The overall working process of the LoC sensor is shown in Fig. 6.

A. Blood Group Identification

For blood group detection, the RBC sample from blood will be used. Our biosensor, which works on SPR, can detect

TABLE II
VALUES OF THE COEFFICIENTS

Coefficient	Unit	Blood Group		
		A	B	O
n_0	-	1.54712	1.54712	1.54712
A	L/g	9.014×10^{-4}	11.09×10^{-4}	11.26×10^{-4}
C	g/L	150.2	140.4	135.33
D	K^{-1}	6.497×10^{-5}	6.497×10^{-5}	6.497×10^{-5}
F_1	nm^{-1}	12.927×10^{-4}	9.79×10^{-4}	12.174×10^{-4}
F_2	nm	29.7629	9.9374	25.4616
F_3	nm^{-2}	1.3958×10^{-6}	9.2945×10^{-7}	1.3125×10^{-6}
F_4	nm^{-4}	4.4578×10^{-13}	2.5922×10^{-13}	4.23×10^{-13}

TABLE III
DETECTION OF BLOOD GROUP

Blood Group	Transmission Dip (dB)	Resonant Wavelength (nm)
A	-16.7712	824.016
B	-16.7183	823.429
O	-16.9755	825.924

various biological parameters, such as glucose, hemoglobin, DNA, and RNA, with high efficiency. It is proposed as an ideal candidate for detecting quantities dependent on RI changes, such as human blood group identification, with Li et al. [25] developing a Cauchy formula based on experimental results for three blood groups at visible and NIR wavelengths. Our proposed sensor functions within the wavelength range of 790–850 nm, where the resonances corresponding to each blood group fall between 815 and 835 nm. Thus, our sensor operates in alignment with the experimental findings reported by Li et al. [25], enabling accurate classification of blood groups based on their RI characteristics

$$n(\lambda)|_j = 1.357 + \frac{A}{\lambda^2} + \frac{B}{\lambda^4}. \quad (14)$$

Here, different blood samples denoted by subscripts *A*, *O*, and *B*, with λ representing the wavelength (nm), the Cauchy coefficients *A* and *B* assume distinct values corresponding to each blood group. The variation of RI for different values of concentration is shown in Fig. 7. To demonstrate variations for different blood groups, we presented concentration vs RI plots at a wavelength of 775 nm. The RI exhibits a nonlinear variation across different wavelengths for blood groups *A*, *B*, and *O* shown in Fig. 8(a). Notably, there is a decrease in RI as wavelength increases, a distinctive feature of human blood groups. Apart from wavelength, RI is influenced by hemoglobin concentration and temperature [8]. Consequently, considering these factors, the formula for blood group RI can be calculated to the following expression [8]:

$$n = n_0 + A \times C + D \times T + \left(F_1 \lambda + \frac{F_2}{\lambda} \right) + F_3 \lambda^2 + F_4 \lambda^4. \quad (15)$$

The formula involves variables such as *C* (mass fraction of dry hemoglobin in g/L), and *T* (temperature in Kelvin). *A* and *D* represent the concentration and temperature coefficients of RI of hemoglobin, respectively. The interplay of RI, hemoglobin concentration, temperature, and wavelength contributes to the variations in blood properties. Notably, the RI differences among blood groups (*A*, *B*, and *O*) affect the λ_{res} . Table II summarizes the parameters employed in our

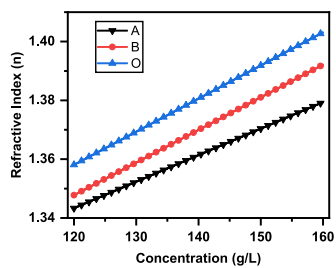


Fig. 7. Relationship between concentration and RI at wavelength, $\lambda = 775$ nm.

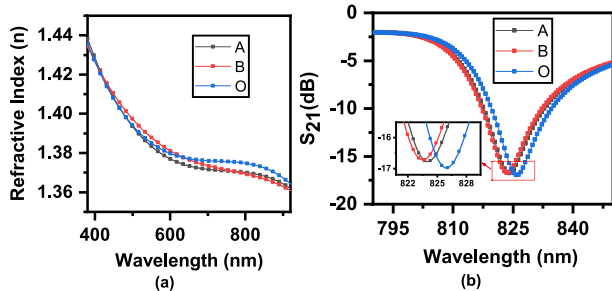


Fig. 8. (a) Wavelength-dependent RI. (b) TC for different blood groups.

simulation of RI for various blood groups at room temperature. Fig. 8(b) depicts the TC of multiple blood groups. The corresponding λ_{res} are specific to each blood group, as obtained through the simulation, and are detailed in Table III. As the designed sensor possesses a detection limit of 1.1548×10^{-6} RIU, it enables precise identification of λ_{res} associated with different blood groups. Utilizing an OSA connected to the ports facilitates accurate detection of these λ_{res} , thereby enabling effective classification of blood groups based on spectral characteristics.

B. Diabetes Level Detection

Detecting diabetes relies on monitoring blood glucose levels, indicative of the condition characterized by elevated glucose. Glucose concentration, the total quantity in a specific blood volume, is crucial for assessing the body's ability to regulate energy [18]. The number of glucose levels and their variability throughout the day, underscoring the importance of an equation for calculating glucose concentration percentage [26]

$$n = 0.2015 \times C\% + 1.3292. \quad (16)$$

Here, “ n ” represents the RI, while “ $C\%$ ” denotes the percentage of glucose concentration. Fig. 9(a) illustrates the changes in TC, and Fig. 9(b) demonstrates the linear correlation between the λ_{res} and glucose concentration.

Our approach offers a systematic method for determining glucose concentration and assessing diabetes levels. Utilizing a specific relationship, the unknown concentration is calculated and converted to mmol/L, enabling a quick evaluation. Molecular weight (MW) and solution density are essential for accurate conversion. Under standard conditions, pure glucose has a density (D) of 1.54 g/mL and a MW of 180.16 g/mol. The mathematical relationship for determining diabetes levels

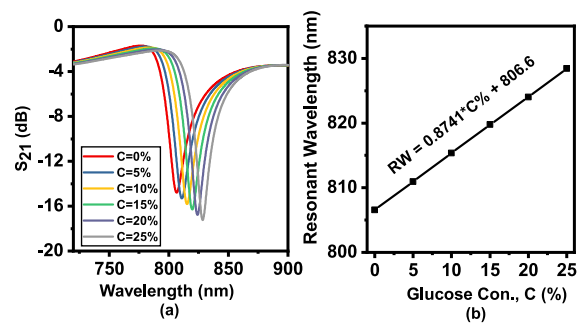


Fig. 9. (a) TC for different glucose concentration. (b) Relationship between resonant wavelength (λ_{res}) and glucose concentration.

can be expressed as follows:

$$\text{Diabetes level} = \frac{\text{Conc.\%} \times D \times 1000}{\text{MW}}. \quad (17)$$

In (17), mmol/L values indicate diabetes levels, which may be used to evaluate whether a person is healthy (< 7.8 mmol/L), prediabetic (7.8–11 mmol/L) or has diabetes (> 11 mmol/L) [26].

IV. CONCLUSION

In this article, we propose a novel demultiplexer-based MIM LoC sensor designed for monitoring human blood groups (A, B, and O) and diabetes levels. The sensor's efficacy is enhanced through the incorporation of a subwavelength silicon diamond-shaped array at the operational wavelength. To prevent cross-contamination, we can detect the two different analytes from two output ports using the demultiplexer feature. To the best of the authors' knowledge, this is the first MIM LoC biosensor reported utilizing a 1×2 demultiplexer. Utilizing the COMSOL Multiphysics software and the FEM analysis, we optimized the sensor parameters, achieving a maximum sensitivity of 865.9 nm/RIU and a FOM of 58.4. This LoC sensor's development and implementation mark a significant advancement in medical diagnostics and personalized medicine, leveraging the latest microfluidic technology and advanced blood group detection methods. Additionally, the sensor provides valuable information on diabetes levels, contributing to the evaluation of an individual's diabetic status.

REFERENCES

- [1] S. K. Sahu and M. Singh, “Plasmonic elliptical nanohole array for on-chip human blood group detection,” *IEEE Sensors J.*, vol. 23, no. 22, pp. 27224–27230, Nov. 2023.
- [2] T. Dar, J. Homola, B. M. A. Rahman, and M. Rajarajan, “Label-free slot-waveguide biosensor for the detection of DNA hybridization,” *Appl. Opt.*, vol. 51, no. 34, p. 8195, Nov. 2012.
- [3] Z. Vafapour, “Polarization-independent perfect optical metamaterial absorber as a glucose sensor in food industry applications,” *IEEE Trans. Nanobiosci.*, vol. 18, no. 4, pp. 622–627, Oct. 2019.
- [4] J. Zhang, L. Zhang, and W. Xu, “Surface plasmon polaritons: Physics and applications,” *J. Phys. D, Appl. Phys.*, vol. 45, no. 11, Mar. 2012, Art. no. 113001.
- [5] Md. F. Hassan, R. H. Sagor, M. R. Amin, M. R. Islam, and M. S. Alam, “Point of care detection of blood electrolytes and glucose utilizing nano-dot enhanced plasmonic biosensor,” *IEEE Sensors J.*, vol. 21, no. 16, pp. 17749–17757, Aug. 2021.
- [6] M. A. A. Butt and N. Kazanskiy, “Enhancing the sensitivity of a standard plasmonic MIM square ring resonator by incorporating the nano-dots in the cavity,” *Photon. Lett. Poland*, vol. 12, no. 1, p. 1, Mar. 2020.

- [7] Y. Tang et al., "Refractive index sensor based on Fano resonances in metal-insulator-metal waveguides coupled with resonators," *Sensors*, vol. 17, no. 4, p. 784, Apr. 2017.
- [8] R. H. Sagor, M. F. Hassan, S. Sharmin, T. Z. Adry, and M. A. R. Emon, "Numerical investigation of an optimized plasmonic on-chip refractive index sensor for temperature and blood group detection," *Results Phys.*, vol. 19, Dec. 2020, Art. no. 103611.
- [9] M. A. Butt, N. L. Kazanskiy, and S. N. Khonina, "Metal-insulator-metal waveguide plasmonic sensor system for refractive index sensing applications," *Adv. Photon. Res.*, vol. 4, no. 7, Jul. 2023, Art. no. 2300079.
- [10] G. Knapp and P. Schramel, "Sources of analyte contamination and loss during the analytical process," *Comprehensive Anal. Chem.*, vol. 41, pp. 23–45, Jan. 2003.
- [11] M. R. Rakhshani and M. A. Mansouri-Birjandi, "High sensitivity plasmonic refractive index sensing and its application for human blood group identification," *Sens. Actuators B, Chem.*, vol. 249, pp. 168–176, Oct. 2017.
- [12] M. A. Butt, S. N. Khonina, and N. L. Kazanskiy, "An array of nanodots loaded MIM square ring resonator with enhanced sensitivity at NIR wavelength range," *Optik*, vol. 202, Feb. 2020, Art. no. 163655.
- [13] N. A. Cinel, S. Büttün, and E. Özbay, "Electron beam lithography designed silver nano-disks used as label free nano-biosensors based on localized surface plasmon resonance," *Opt. Exp.*, vol. 20, no. 3, p. 2587, Jan. 2012.
- [14] A. Bhukta, S. Ravulapalli, and P. V. Satyam, "Comparative inter diffusion study among Ag and AuAg thin film grown on reconstructed Si(5 12) substrate," *Appl. Phys. A, Solids Surf.*, vol. 128, no. 1, p. 66, Jan. 2022.
- [15] P. B. Johnson and R. W. Christy, "Optical constants of the noble metals," *Phys. Rev. B, Condens. Matter*, vol. 6, no. 12, pp. 4370–4379, Dec. 1972.
- [16] R. H. Sagor, M. F. Hassan, A. A. Yaseer, E. Surid, and M. I. Ahmed, "Highly sensitive refractive index sensor optimized for blood group sensing utilizing the Fano resonance," *Appl. Nanoscience*, vol. 11, no. 2, pp. 521–534, Feb. 2021.
- [17] J. Wu, P. Lang, X. Chen, and R. Zhang, "A novel optical pressure sensor based on surface plasmon polariton resonator," *J. Modern Opt.*, vol. 63, no. 3, pp. 219–223, Feb. 2016.
- [18] M. R. Rakhshani, A. Tavousi, and M. A. Mansouri-Birjandi, "Design of a plasmonic sensor based on a square array of nanorods and two slot cavities with a high figure of merit for glucose concentration monitoring," *Appl. Opt.*, vol. 57, no. 27, p. 7798, Sep. 2018.
- [19] M. Danaie and A. Geravand, "Design of low-cross-talk metal-insulator-metal plasmonic waveguide intersections based on proposed cross-shaped resonators," *Proc. SPIE*, vol. 12, no. 4, Oct. 2018, Art. no. 046009.
- [20] T. J.-Y. Derrien, J. Krüger, and J. Bonse, "Properties of surface plasmon polaritons on lossy materials: Lifetimes, periods and excitation conditions," *J. Opt.*, vol. 18, no. 11, Nov. 2016, Art. no. 115007.
- [21] K. V. Voronin, Y. V. Stebunov, A. A. Voronov, A. V. Arsenin, and V. S. Volkov, "Vertically coupled plasmonic racetrack ring resonator for biosensor applications," *Sensors*, vol. 20, no. 1, p. 203, Dec. 2019, doi: [10.3390/s2010203](https://doi.org/10.3390/s2010203).
- [22] M. G. Blaber, M. D. Arnold, and M. J. Ford, "A review of the optical properties of alloys and intermetallics for plasmonics," *J. Phys., Condens. Matter*, vol. 22, no. 14, Apr. 2010, Art. no. 143201.
- [23] W. L. Barnes, "Surface plasmon-polariton length scales: A route to sub-wavelength optics," *J. Opt. A, Pure Appl. Opt.*, vol. 8, no. 4, pp. 87–93, Apr. 2006.
- [24] M. A. Butt, "Plasmonic sensor realized on metal-insulator-metal waveguide configuration for refractive index detection," *Photon. Lett. Poland*, vol. 14, no. 1, pp. 1–3, Mar. 2022.
- [25] H. Li, L. Lin, and S. Xie, "Refractive index of human whole blood with different types in the visible and near-infrared ranges," *Proc. SPIE*, vol. 3914, p. 517, Jun. 2000.
- [26] Md. F. Hassan, I. Tathfif, M. Radoan, and R. H. Sagor, "A concentric double-ring resonator based plasmonic refractive index sensor with glucose sensing capability," in *Proc. IEEE REGION 10th Conf. (TENCON)*, Nov. 2020, pp. 91–96.
- [27] H. Chopra, R. S. Kaler, and B. Painam, "Photonic crystal waveguide-based biosensor for detection of diseases," *J. Nanophotonics*, vol. 10, no. 3, Aug. 2016, Art. no. 036011.
- [28] S. Singh and V. Kaur, "Photonic crystal fiber sensor based on sensing ring for different blood components: Design and analysis," in *Proc. 9th Int. Conf. Ubiquitous Future Netw. (ICUFN)*, Jul. 2017, pp. 399–403.
- [29] H. J. El-Khozondar, P. Mahalakshmi, R. J. El-Khozondar, N. R. Ramanujam, I. S. Amiri, and P. Yupapin, "Design of one dimensional refractive index sensor using ternary photonic crystal waveguide for plasma blood samples applications," *Phys. E, Low-Dimensional Syst. Nanostruct.*, vol. 111, pp. 29–36, Jul. 2019.
- [30] A. Bijalwan, B. K. Singh, and V. Rastogi, "Analysis of one-dimensional photonic crystal based sensor for detection of blood plasma and cancer cells," *Optik*, vol. 226, Jan. 2021, Art. no. 165994.
- [31] Z. Chen et al., "A CRISPR/Cas12a-powered surface plasmon resonance platform for rapid and specific diagnosis of the omicron variant of SARS-CoV-2," *Nat. Sci. Rev.*, vol. 9, no. 8, Aug. 2022, Art. no. nwac104.
- [32] F. Zheng et al., "A highly sensitive CRISPR-powered surface plasmon resonance sensor for diagnosis of inherited diseases with femtomolar-level real-time quantification," *Adv. Sci.*, vol. 9, no. 14, May 2022, Art. no. 2105231.
- [33] T. Xue et al., "Ultrasensitive detection of miRNA with an antimonene-based surface plasmon resonance sensor," *Nature Commun.*, vol. 10, no. 1, p. 28, Jan. 2019.
- [34] Z. Chen et al., "CRISPR-Cas13a-powered electrochemical biosensor for the detection of the L452R mutation in clinical samples of SARS-CoV-2 variants," *J. Nanobiotechnol.*, vol. 21, no. 1, p. 141, Apr. 2023.
- [35] D. Qu, Q. Wu, Y. Sun, and C. Li, "Research on high sensitivity Fano resonance sensing based on MIM waveguide coupled with double Fibonacci spirals," *J. Comput. Electron.*, vol. 22, no. 5, pp. 1500–1506, Oct. 2023.
- [36] D. Qu, Q. Wu, Y. Sun, and C. Li, "Research on highly sensitive and independently tunable sensing in MIM waveguide structure based on Fano resonance," *J. Opt.*, vol. 53, no. 1, pp. 389–395, Apr. 2023.
- [37] D. Qu, Y. Sun, Y. Ren, Q. Wu, and C. Li, "Research on sensing characteristics of triple independent tuning with high sensitivity based on MIM waveguide," *Opt. Quantum Electron.*, vol. 56, no. 2, p. 137, Feb. 2024.
- [38] Y. Sun, D. Qu, Q. Wu, and C. Li, "MIM plasmonic sensors based on single-side ring cavity with one stub and their applications," *Phys. Scripta*, vol. 99, no. 2, Feb. 2024, Art. no. 025506.
- [39] S. T. Foroughi, R. Yadipour, S. Golmohammadi, and T. Nurmoohammadi, "Slow light realization based on plasmon-induced transparency in Γ-shaped rectangular resonator structures," *Plasmonics*, pp. 1–7, Sep. 2023.
- [40] A. Kuzma et al., "Influence of surface oxidation on plasmon resonance in monolayer of gold and silver nanoparticles," *J. Appl. Phys.*, vol. 112, no. 10, Nov. 2012.
- [41] M. Danaie and A. Shahzadi, "Design of a high-resolution metal-insulator-metal plasmonic refractive index sensor based on a ring-shaped Si resonator," *Plasmonics*, vol. 14, no. 6, pp. 1453–1465, Dec. 2019.
- [42] I. Tathfif, A. A. Yaseer, K. S. Rashid, and R. H. Sagor, "Metal-insulator-metal waveguide-based optical pressure sensor embedded with arrays of silver nanorods," *Opt. Exp.*, vol. 29, no. 20, p. 32365, Sep. 2021.
- [43] D. Murra, S. Bollanti, P. Di Lazzaro, F. Flora, and L. Mezi, "Interfacing Arduino boards with optical sensor arrays: Overview and realization of an accurate solar compass," *Sensors*, vol. 23, no. 24, p. 9787, Dec. 2023.
- [44] J. Stanley and N. Pourmand, "Nanopipettes—The past and the present," *APL Mater.*, vol. 8, no. 10, Oct. 2020, Art. no. 100902.
- [45] Q. Zhang, X.-G. Huang, X.-S. Lin, J. Tao, and X.-P. Jin, "A sub-wavelength coupler-type MIM optical filter," *Opt. Exp.*, vol. 17, no. 9, p. 7549, Apr. 2009.



Rummanur Rahad (Member, IEEE) received the B.Sc. degree in electrical and electronic engineering from the Islamic University of Technology (IUT), Gazipur, Bangladesh, in 2023.

He was a part-time Lecturer at IUT and plays an integral role as an Active Researcher at IUT Photonics Research Group (IUTPRG). He is currently working as a Research Assistant (RA) at the Optics and Photonics Research Group, BRAC University, Dhaka, Bangladesh. He has authored several research papers in renowned journals such as *Optics Express*, *Results in Physics*, *Sensing and Bio-Sensing Research*, and *Optics Communications*. His research interests include optical devices, bio-photonics, metamaterials, and solar cells.



Mohammad Ashraful Haque received the B.Sc. degree in electrical and electronic engineering from the Islamic University of Technology, Gazipur, Bangladesh, in 2023.

He is a former Team Lead with IUT Mars Rover–Team Avijatrik, Gazipur. He is also a member with the IUT Photonics Research Group (IUTPRG). He has authored or coauthored reputable journals, such as *Result in Physics*, *Sensing Bio-Sensing Research*, and *Optics Communications*. His research interests include encompass optical sensors and devices, metamaterials, robotics, the Internet of Things (IoT), and autonomous navigation.



Md Sadi Mobassir is currently pursuing the B.Sc. degree in electrical engineering with the Islamic University of Technology (IUT), Gazipur, Bangladesh, with a subsidiary organ of OIC.

He is currently an Electrical Team Lead at Project Altair. His research interests include robotics, electronics, and machine learning.



Md. Omar Faruque received the B.Sc. and M.Sc. degrees in electrical and electronic engineering from the Islamic University of Technology (IUT), Gazipur, Bangladesh, in 2016 and 2019, respectively, with a subsidiary organ of OIC.

He is an Assistant Professor of Electrical and Electronic Engineering at IUT and is currently on leave. He has published 18 scientific research papers in referred journals and conference proceedings. His research interests lie in plasmonic materials and devices.



Abu S. M. Mohsin received the B.Sc. degree in electrical and electronics engineering (EEE) from the Islamic University of Technology (IUT), Gazipur, Bangladesh, in 2008, and the Ph.D. degree in nanotechnology/nano-biophotonics from the Swinburne University of Technology, Hawthorn, VIC, Australia, in 2015.

From 2011 to 2018, he worked for several departments at the Swinburne University of Technology, in different capacities. He is currently serving as an Associate Professor with BRAC University, Dhaka, Bangladesh. His research interests include nano-bio-photonics, plasmonic nanomaterial, automation, control, and the IoT.



Rakibul Hasan Sagor received the B.Sc. degree in electrical and electronic engineering from the Islamic University of Technology (IUT), Gazipur, Bangladesh, in 2007, the M.Sc. degree in electrical engineering from the King Fahd University of Petroleum and Minerals (KFUPM), Dhahran, Saudi Arabia, in 2011, and the Ph.D. degree in electrical and electronic engineering from IUT, in 2018.

He is currently serving as a Professor with IUT and he is a Research Coordinator of IUT Photonics Research Group (IUTPRG). He specializes in photonics, plasmonics, and high-power microwave. He has contributed significantly to his field with 85 research papers published in various journals and conference proceedings.